JOURNAL OF CATALYSIS **167,** 164–171 (1997)
ARTICLE NO. CA971559

Catalytic Properties of $Bi_4V_{2-x}Sb_xO_{11-\delta}$ in Methanol Oxidation

H. R. Aghabozorg,* W. R. Flavell,* and B. H. Sakakini†

*Department of Physics and †Department of Chemistry, UMIST, P.O. Box 88, Manchester M60 1QD, United Kingdom

Received July 31, 1996; revised November 21, 1996; accepted November 28, 1996

Ceramic model catalysts of general formula $Bi_4V_{2-x}Sb_xO_{11-\delta}$ are synthesised by solid-state reaction. X-ray diffraction shows the materials to be single phase over the composition range $0 \leq x < 0.3$, with a second phase, which is not identified, produced at higher antimony doping level. XPS results show oxidation states of +IV and +V for vanadium in these compounds. These results also indicate that the proportion of antimony on the surface of the compounds is greater than that in the bulk of these compounds. The catalytic properties of the materials are examined using methanol oxidation as a test reaction. The activity and selectivity to formaldehyde production shown by these materials is found to be strongly correlated with the antimony doping level.

INTRODUCTION

It is well known that Bi_2O_3 exhibits a remarkable range of useful solid-state properties (1). Many multicomponent systems containing ternary oxides of Bi, such as bismuth vanadium molybdenum oxides (for example, $BiMo_{1-x}V_xO_4$) or the various types of bismuth molybdates (Bi_2MoO_6, $Bi_2Mo_2O_9$, and $Bi_2Mo_3O_{12}$), are efficient selective oxidation catalysts for hydrocarbons. Structural oxygen is released from the catalyst, thereby converting it to a nonstoichiometric solid. The anion deficiency is made good when reactant gaseous oxygen is taken up by the catalyst, in a Mars–van Krevelen mechanism (20).

The bismuth-containing layered perovskite-like compound, which was studied by Kargin (3), corresponds to the general crystallochemical formula, $(Bi_2O_2)^{2+}$ $(A_{n-1}B_n \cdot O_{3n+1})^{2-}$ belonging to Aurivillius phases (B denotes Ti^{4+}, Ta^{5+}, Nb^{5+}, W^{6+}, and other ions capable of forming oxygen octahedra; A denotes Bi^{3+}, Ba^{2+}, Pb^{2+}, Sr^{2+}, Ca^{2+}, and other ions with corresponding sizes; $n = 1, 2, 3, \ldots$ is the number of perovskite-like layers between the bismuthyl layers, $(Bi_2O_2)^{2+}$). Complex perovskite and layered perovskite metal oxides are of considerable interest, as their properties may be tailored to specific applications by subtle changes in chemical doping at the A or B cation sites.

Barrault *et al.* (4) studied the oxidative coupling of methane in the presence of $(Bi_2O_2)^{2+}(A_{n-1}B_nO_{3n+1})^{2-}$ (A denotes Ca, Sr, Ba, and Pb, and B denotes Nb and Ta). Their results showed that these materials are selective and stable in the aforementioned reaction. Moreover, their substitution in perovskite (A) or octahedral (B) sites leads to significant change of the C^{2+} selectivity or yield which is attributed to modification of the basicity of A–O or B–O bonds.

The compound $Bi_2VO_{5.5}$ (or $Bi_4V_2O_{11}$), in which all positions of the B sublattice are occupied by V^{5+} ions only, while the A sublattice for compositions with $n = 1$, is absent, was also synthesised (5). Preparation and characterisation of doped $Bi_4V_2O_{11}$ materials have been studied by many authors (6–10). Joubert *et al.* attempted to dope antimony into the V site in this compound leading to preparation and characterisation of $Bi_4V_{1.5}Sb_{0.5}O_{10.7}$ (9).

Vanadium–antimony oxides have been developed as catalysts for the oxidation of hydrocarbons (11–16). Berry and Brett (11) investigated the properties of vanadium–antimony oxide catalysts. Their results were consistent with the reduction of the catalyst during the catalytic reaction and more specifically, with the reduction of vanadium (IV) in the oxidised vanadium antimonate phase ($VSbO_4$). Nilsson *et al.* prepared V–Sb–O catalysts with different Sb : V ratios and used them for the ammoxidations of propane and propylene (12).

In the current work $Bi_4V_{2-x}Sb_xO_{11-\delta}$ compounds are prepared over the nominal range $0 \leq x \leq 1.7$ and the catalytic behaviour of these compounds is studied using methanol oxidation as a simple test reaction. The production of formaldehyde is used as a measure of selectivity to partial oxidation, while production of CO_2 is used to monitor deep oxidation.

EXPERIMENTAL

Ceramic samples of nominal formula $Bi_4V_{2-x}Sb_xO_{11-\delta}$ were prepared by solid-state reaction. Stoichiometric amounts of Bi_2O_3, V_2O_5, and Sb_2O_3 were ground to constant particle size using a vibrating agate ball mill, and the green mix was slowly annealed (1°C/min) in air up to 1073 K. After annealing for 4 h at this temperature, it was slowly cooled (1°C/min) to room temperature.

X-ray diffraction (XRD) was carried out using a Philips Horizontal Powder Diffractometer and monochromated Cu $K\alpha$ radiation. X-ray photoelectron spectroscopy (XPS)

0021-9517/97 $25.00

was carried out using a Fison's Instruments XR3 twin anode X-ray gun and CLAM2 hemispherical analyser, in an ion-pumped chamber. In this case powder samples were loaded onto Cu plates. Argon ion etching was achieved using a PSP Instruments ISIS3000 filament Ar^+ ion gun.

The surface areas of the catalyst were measured by the BET method using nitrogen. In the methanol oxidation studies, a continuous flow system was used. One-gram quantities of catalysts were loaded onto glass wool in a 1-cm-diameter quartz reactor, which was located in a temperature-controlled furnace. The thermocouple was adjacent to the sample position in the furnace. Methanol was introduced by bubbling dry He through a glass saturator filled with methanol. The total flow rate of dry O_2, He/MeOH, and He above the catalyst was controlled using a vent valve before the reactor and measured by a bubble flow meter after the reactor. The product gases were sampled immediately after the reactor and were injected into a gas chromatograph provided with a thermal conductivity detector (TCD) for analysis. O_2, CO_2, HCHO, H_2O, and MeOH were separated using a Propack-T column. To prevent condensation of reactant and product gases the tubing between the saturator and the sampling valve, and between the reactor and the bubble flow meter, was heated to 373–383 K. The catalysts were pretreated at 723 K in 1 : 1 He/O_2 for 16 h, followed by flushing with He for 10 min. To investigate the effect of different pretreatments on the catalytic behaviour, catalysts were also pretreated in pure He at 723 K for 16 h. The reaction was carried out at temperatures in the range 523–623 K. After establishing steady-state conditions (around 30 min in reactant flow), the reaction products were analysed at a constant flow rate of 52 ml min^{-1}. For each catalyst material and each pretreatment at least three experimental runs were made, and measurements were taken as the temperature was raised. In order to check that these measurements were not affected by any time-dependent poisoning effect, for selected materials the measurements were rechecked as the temperature was lowered. No significant changes were noted. To investigate the effect of catalytic reaction on the catalysts, selected samples were cooled to room temperature after catalytic reaction under both He/O_2 and He streams. The random error associated with averaged readings taken for each sample is estimated to be $\leq \pm 3\%$. This gives relative values of percentage of selectivity and percentage of total conversion (Table 3) which are reproducible to within $\leq \pm 5\%$.

RESULTS AND DISCUSSION

Sample Characterisation

Powder XRD patterns for various values of the antimony doping level, x, are shown in Fig. 1. In the doping range $0 \leq x < 0.3$, the samples appeared single phase, and reflections were indexed using the standard JCPDS file (No. 42-349) for $Bi_4V_2O_{11}$. For samples with $x \geq 0.3$ some doublet peaks convert to single peaks which could be consistent with transformation of the structure from orthorhombic to tetragonal, e.g., the peaks at 32° and 32.4° corresponding to (020) and (200) reflections, respectively, convert to a single peak at 32.3°. This is in agreement with the lattice parameters of the unit cell in these compounds which are shown in Table 1. On increasing the doping level a decreases and at $x = 0.3$, $a = b = 5.5324$ Å and $c = 15.4596$ Å. For samples with $x \geq 0.3$ a secondary phase, which is not identified, was observed, as shown in Fig. 1. This behaviour (a transition from orthorhombic to tetragonal) has been reported for $Bi_4V_2O_{11}$ and $Bi_2V_{1-x}M_xO_{5.5-3x/2}$ compounds (where M is Cu and Ni) by Bhattacharya *et al.* (31) and Abraham *et al.* (7, 32), respectively. The $Bi_2V_{1-x}Cu_xO_{5.5-3x/2}$ compounds in the range $0 \leq x \leq 0.07$ are orthorhombic, but for the range

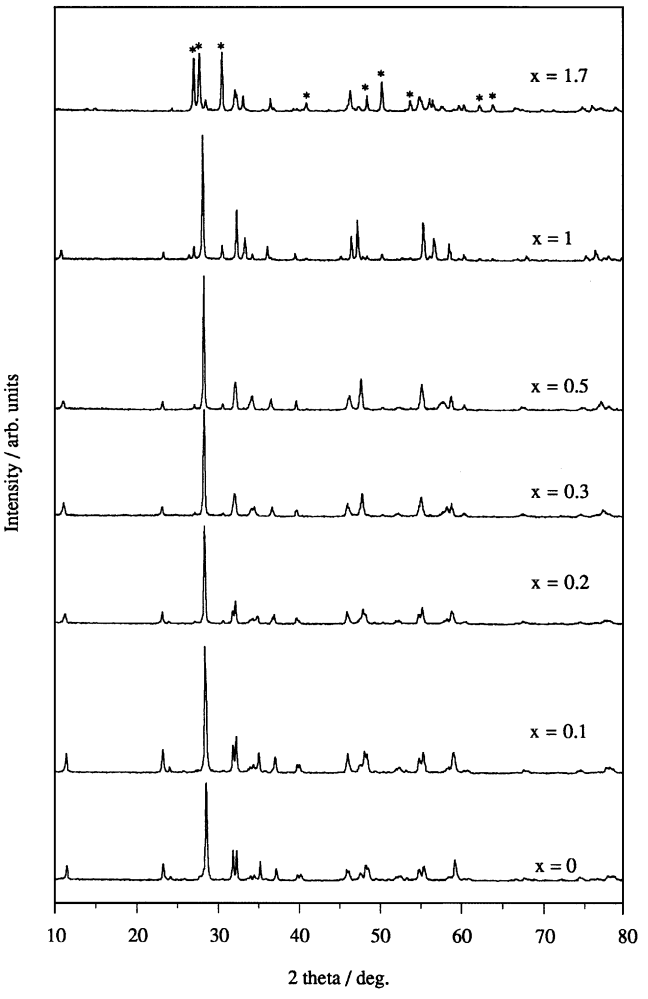

FIG. 1. Powder XRD patterns for the $Bi_4V_{2-x}Sb_xO_{11-\delta}$ compounds ($x = 0$, 0.1, 0.2, 0.3, 0.5, 1, 1.7), showing the appearance of the second phase as a function of Sb doping level, and the disappearance of the orthorhombic distortion, as evidenced by the coalescence of the (020) and (200) reflections at $2\theta = 32°$ and 32.4°, respectively. Peaks due to the second phase appearing for $x > 0.2$ are indicated by asterisks.

TABLE 1

Cell Dimensions of $Bi_4V_{2-x}Sb_xO_{11-\delta}$ Compounds from XRD

x	a/Å	b/Å	c/Å	Volume/Å^3
0	5.516	5.595	15.220	469.74
0.06	5.522	5.598	15.272	472.09
0.1	5.521	5.588	15.286	471.58
0.2	5.522	5.586	15.315	472.41
0.3	5.532	—	15.460	473.18
0.5	5.524	—	15.596	475.93
1	5.483	—	15.553	467.63
1.7	5.463	—	14.620	436.38

$0.07 \leq x \leq 0.12$, the room-temperature unit cell is tetragonal. The Ni-substituted compounds with $x = 0.07$ show that this compound has a tetragonal structure.

In Fig. 2, XRD patterns recorded for a sample having $x = 0.2$, which is cooled to room temperature under different streams (He and He/O_2), after catalytic reaction are compared with the XRD pattern of the same sample before reaction (for reasons of clarity, the patterns are only shown from the Bragg angle, 2θ, 30° to 35°). For the sample which is cooled under He alone the doublet peaks corresponding to the (020) and (200) reflections appear to be converted to one single (200) reflection, but after cooling under the He/O_2 stream the doublet peaks are again observed. This comparison suggests that the structure might convert from orthorhombic to tetragonal during the catalytic reaction, but under a He/O_2 stream the catalyst can reconstruct to the orthorhombic structure again.

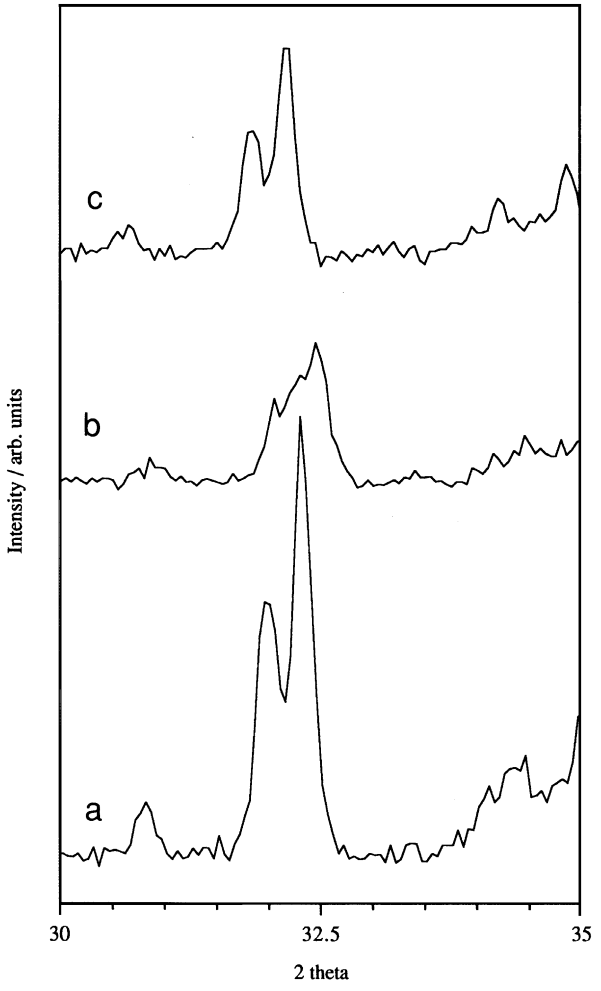

FIG. 2. Powder XRD patterns recorded for the $Bi_4V_{1.8}Sb_{0.2}O_{11-\delta}$ samples. (a) Before reaction; (b) after reaction cooled to room temperature under He stream; and (c) after reaction cooled to room temperature under He/O_2 stream.

As might be expected from the high annealing temperatures used to synthesise these "model catalyst" materials, the samples were highly crystalline, as evidenced by the narrow reflections observed in XRD. Consistent with this, the BET surface areas were much lower than in a normal working catalyst material, typically in the range 0.3–0.7 $m^2\ g^{-1}$, and these showed small random fluctuation with Sb doping level. We note that the values obtained via this route for powders with surface areas $<1\ m^2\ g^{-1}$ may be subject to errors of around ±25%, so these measurements merely indicate a low and roughly constant surface area.

The surface chemical composition of the samples was checked by performing XPS over a range of binding energies. The experiment was carried out before and after performing the catalytic reaction on the catalysts. Examination of the carbon 1*s* region from uncleaned samples indicated a signal that could be assigned to hydrocarbon. After argon ion etching the samples, this signal was removed. In order to calibrate the energy scale in an XPS study of the oxides of vanadium, Mendialdua *et al.* suggested that the best energy reference for this purpose is the O1*s* level (17). Therefore, in this work the O1*s* level has been used as calibrant and it was assumed that the aforementioned level is at 531 eV. The O1*s* peak overlaps the region in which the most intense peak for antimony ($Sb3d_{5/2}$) should appear. Therefore, the presence of antimony on the surface of samples should be probed by the $Sb3d_{3/2}$ peak. In addition, concerning vanadium, only the $V2p_{3/2}$ component can be accurately treated because the $V2p_{1/2}$ peak overlaps with the O1*s* $K\alpha_{3,4}$ satellite peak. The problems associated with the deconvolution of partially overlapping weak signals, combined with some difficulties associated with sample charging, mean that absolute quantification of these data must be approached with caution. However, calculations of surface chemical composition (Table 2) show that the proportion of antimony on the surface of the compounds is more than that in the bulk of these compounds. This trend is more evident for lower antimony doping level, x, and it seems that the Sb concentration in the surface layers of the vanadate may be approaching some limiting value when the bulk doping level increases. In addition, the XPS results show that the proportion of antimony after performing the

TABLE 2

The Bulk Nominal and Experimentally Determined Surface Concentration Ratios of Antimony and Total Vanadium, N(Sb) : N(V), and the Ratio of Vanadium Oxidation States, V^{IV} : V^{V}

	Surface experimental					
		N(Sb) : N(V)				
	V^{IV} : V^{V}			Before reaction (etched sample)	After reaction (etched sample)	
x	Before reaction	Before reaction	After reaction			Bulk nominal
0	0.6	—	—	—	—	0
0.06	0.2	—[a]	—[a]	0.23	—[a]	0.03
0.1	0.3	0.07	0.11	0.15	0.13	0.05
0.5	0.6	—	0.36	0.49	0.37	0.33

Note. Estimated error ±20%.
[a] Indicates Sb level too low for quantification.

catalytic reaction increases on the surface of as-presented samples. This may indicate a possible reconstruction of the surface of nominally orthorhombic samples to tetragonal during the catalytic reaction, in line with XRD results that indicate the reconstruction of the bulk of the samples to tetragonal is associated with increasing the antimony doping level. (Our XRD results indicate that the bulk transition occurs between $x = 0.2$ [N(Sb) : N(V) = 0.11] and $x = 0.3$ [N(Sb) : N(V) = 0.18].) The surface experimental Sb : V ratio from XPS is compared with the bulk nominal ratio in Table 2, from which it can be seen that the surface Sb concentration exceeds these values for very low values of the nominal Sb doping level. On fitting the V2$p_{3/2}$ peak by means of two components (e.g., Fig. 3a), it is clear that the first one at 516.8 eV is characteristic of V^V, whereas the second one at 518 eV can be assigned to V^{IV}. This is in agreement with the results of Joubert *et al.* on the XPS of the $Bi_4V_{1.5}Sb_{0.5}O_{10.7}$ compound (9), where a peak separation of 1.2 eV between the two oxidation states is also observed. This behaviour suggests flexible redox behaviour at the surface of these compounds. The surface V^{IV} : V^V ratio shows a somewhat erratic variation with x (antimony doping level). We note that this ratio will be subject to a high error, as it involves fitting and taking a ratio between two weak, overlapping signals. Nevertheless, the values are roughly consistent with the ratio of 0.66 estimated by Joubert *et al.* for $Bi_4V_{1.5}Sb_{0.5}O_{10.7}$ ($x = 0.5$) (9). There is some suggestion from the data that the V^{IV} : V^V ratio increases with Sb concentration for the Sb-doped samples. The binding energy of the maximum intensity point of the V2$p_{3/2}$ peak from the samples decreases by 0.3–0.9 eV after performing catalytic reaction on them. This behaviour could show a reduction in vanadium oxidation state during catalytic reaction. In other words, it could be concluded that the catalytic redox cycle involves reduction of V^V to a lower oxidation state. This is modelled in our XPS measurements by light Ar^+ ion etching. Surface cleaning under Ar^+ induces a reduction especially of V^V on the surface of the samples. The curve-fitted V2$p_{3/2}$ spectrum of a Sb-doped sample ($x = 0.1$), after etching by Ar^+, is compared with the V2$p_{3/2}$ spectrum before Ar^+ etching in Fig. 3. The FWHM (full width at half maximum) for the components becomes larger after etching, which is probably associated with the surface damage caused by etching.

Catalytic Measurements

For each catalyst material, Arrhenius plots were constructed for partial (production of HCHO), deep (production of CO_2), and total (CO_2 + HCHO) oxidation,

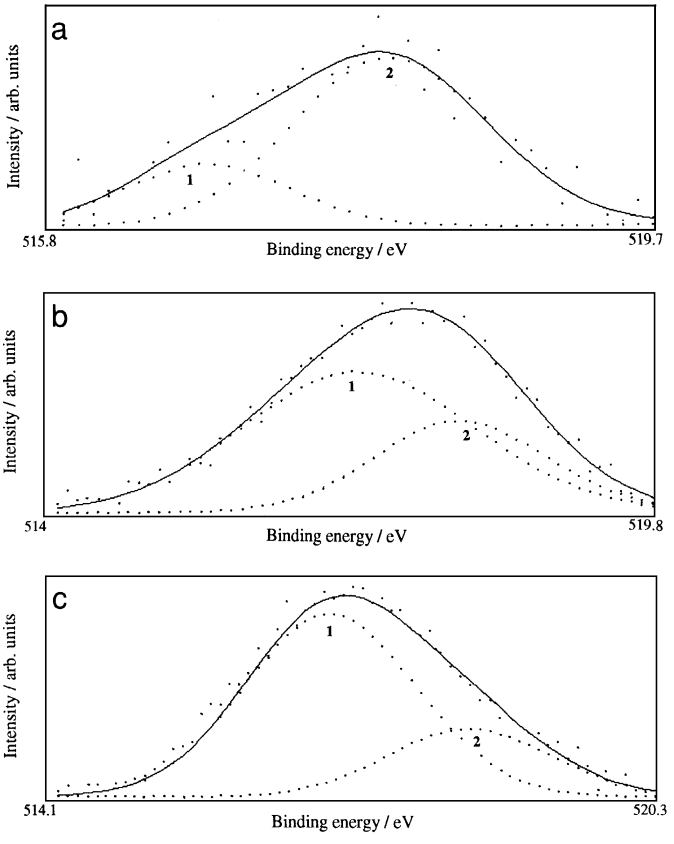

FIG. 3. Curve-fitted V2$p_{3/2}$ spectra of a $Bi_4V_{1.9}Sb_{0.1}O_{11-\delta}$ sample. (a) Before argon ion etching; (b) after argon ion etching for ~20 min; and (c) after argon ion etching for a further ~20 min. Peak fitting parameters (in particular the energy separation of the components) is based on the work of Joubert *et al.* (9). Fitting parameters:

	Peak position 1/eV	FWHM/eV	Area/cps	Peak position 2/eV	FWHM/eV	Area/cps
(a)	516.8	1.3	130.9	518	1.5	421.2
(b)	516.9	2.7	1324.7	517.9	2	634.8
(c)	516.9	2.1	1816.5	518.4	2	635.9

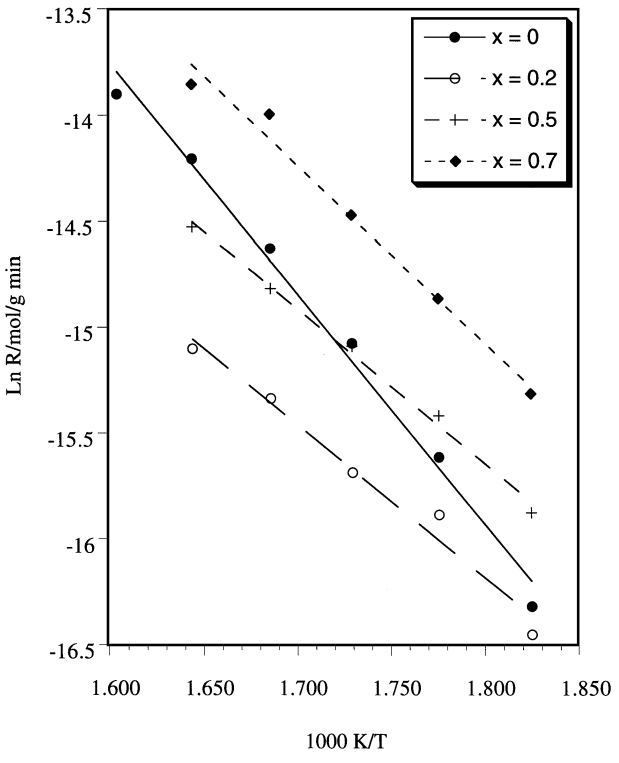

FIG. 4. Selected Arrhenius plots of total oxidation for He/O_2 pretreatment.

after He pretreatment and He/O_2 pretreatment over the temperature range 523–623 K. Selected Arrhenius plots for total oxidation are compared in Fig. 4. It was assumed that the rate law does not change with temperature or composition, so that the measured rate of production of products was taken as proportional to rate throughout. In general, good straight-line plots were obtained, allowing the extraction of activation energies for both partial and deep oxidation. For partial oxidation, these are typically in the range ~30–75 kJ mol^{-1}, with higher values, in the range ~50–150 kJ mol^{-1} for deep oxidation. In both cases, the activation energies rise to a maximum at around $x = 0.08$ Sb doping level, and then fall. The values for partial oxidation are low and indicate that the reaction is moving to deep oxidation at higher temperatures. This can be seen in Table 3, which shows a compilation of percentage of conversion and selectivity data for a range of the materials studied.

The total activity of the catalyst materials was not substantially affected by the pretreatment process used. Figure 5 shows the activity of the catalyst materials to production of all products (CO_2 and HCHO) as a function of bulk antimony content, after both He and He/O_2 pretreatment, obtained at temperature 570 K. The data points are taken from the straight-line fits to the relevant Arrhenius plots. Here, activity is normalised in the conventional way to the mass of catalyst (i.e., ln(mol g^{-1} min^{-1})), but normalisation instead to the surface area of the catalyst produces an insignificant change to the overall shape of the plots, as the variations in surface area across the doping range are small and random.

Figure 6 shows the selectivity of the materials to the production of formaldehyde, again as a function of bulk antimony content after He pretreatment and He/O_2 pretreatment. The data in Fig. 6 is presented in the conventional way, maintaining a roughly constant total conversion of <1%. The total conversion obtained from these very low surface area materials is always low. The selectivity of the materials to the production of formaldehyde varies dramatically with temperature and with antimony doping level.

A number of trends emerge from the data. The most dramatic of these, shown clearly in the data of Fig. 5, and reflected in the data at other temperatures, is the drop in activity of the materials as Sb is introduced. This drop in overall activity of the materials is produced mainly by a

TABLE 3

Selectivity to HCHO and Total Conversion in Methanol Oxidation over $Bi_4V_{2-x}Sb_xO_{11-\delta}$ as a Function of Sb Content, Temperature, and Catalyst Pretreatment, for Selected Representative Compositions

		HCHO selectivity/%		Total conversion/%	
x	T/K	He/O_2 Pre.	He Pre.	He/O_2 Pre.	He Pre.
0	548	100.0	—	0.1	—
	563	85.0	100.0	0.2	—
	578	75.6	100.0	0.3	0.1
	593	67.2	74.3	0.4	0.2
	608	61.1	66.4	0.6	0.2
	623	56.1	59.5	0.8	0.3
	638	—	56.4	—	0.5
0.04	563	66.7	100.0	0.1	—
	578	56.8	66.3	0.1	0.1
	593	50.2	54.1	0.2	0.1
	608	42.9	45.9	0.3	0.2
	623	32.6	42.7	0.4	0.3
0.08	548	100.0	—	—	—
	563	100.0	100.0	0.1	—
	578	78.0	76.2	0.1	0.1
	593	71.7	56.7	0.2	0.1
	608	60.3	50.6	0.3	0.2
	623	55.3	46.6	0.5	0.3
0.2	548	61.2	—	0.1	—
	563	49.0	68.4	0.1	0.1
	578	38.4	65.0	0.1	0.1
	593	38.1	64.3	0.2	0.1
	608	35.3	56.4	0.3	0.2
	623	—	53.3	—	0.2
0.7	548	19.4	—	0.2	—
	563	14.5	23.0	0.3	0.2
	578	13.0	19.2	0.5	0.4
	593	8.7	15.0	0.8	0.5
	608	10.0	11.8	0.9	0.7
	623	—	10.2	—	0.9

drop in the rate of production of CO_2. The rate of production of total products decreases when the antimony doping level, x, is in the range $0 \leq x \leq 0.08$. The activity then climbs again, through to the highest doping levels studied. Although around $x = 0.3$, there is a slight drop in the rate of increase, in the range $x > 1$, the total activity of catalysts which contain secondary phase increases sharply. It can also be seen from Fig. 5 that the activity of the He-pretreated materials appears consistently lower than that of the He/O_2 pretreated materials.

Selectivity to production of formaldehyde for the Sb-doped compounds is highest at the lowest temperatures studied, but again appears to show some correlation with antimony content, x. The optimum selectivity to formaldehyde is for the compound containing no antimony (i.e., $x = 0$) and by doping antimony (i.e., increasing x) a drop in selectivity is seen. However, this overall downward trend is interrupted in the range $x = 0.06$–0.08 by a reproducible and apparently anomalous rise in selectivity for both He/O_2 and He pretreatments. Beyond $x = 0.08$, the selectivity of materials decreases dramatically, but it is roughly constant for antimony contents around the range $0.2 < x < 1$. The selectivity increases again after this doping level up to the highest doping level studied.

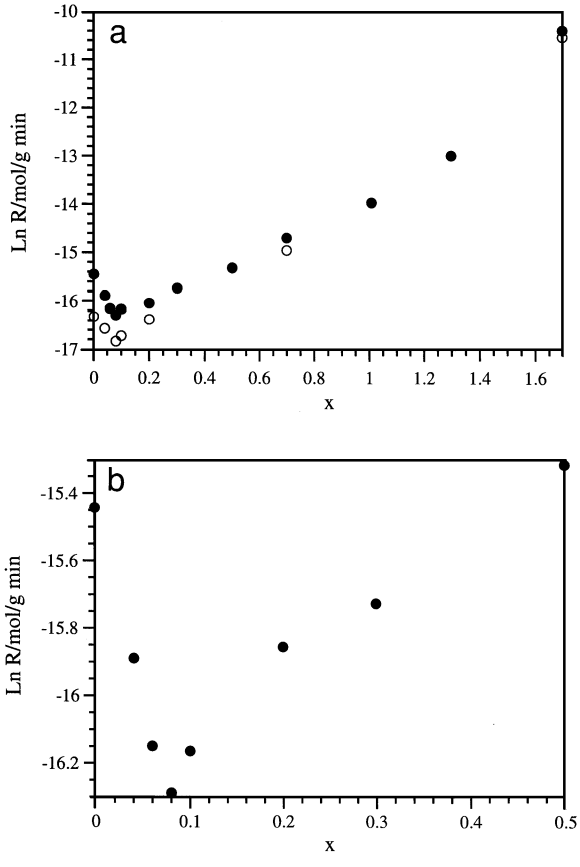

FIG. 5. The effect of Sb doping on the catalyst activity in methanol oxidation [expressed as ln(total moles g^{-1} min^{-1})]. Closed circles represent the total activity of the catalysts after He/O_2 pretreatment and open circles represent the total activity of the catalysts after He pretreatment (a) for a wide range of doping level, $x = 0$–1.7, and (b) expanded region $x = 0$–0.5.

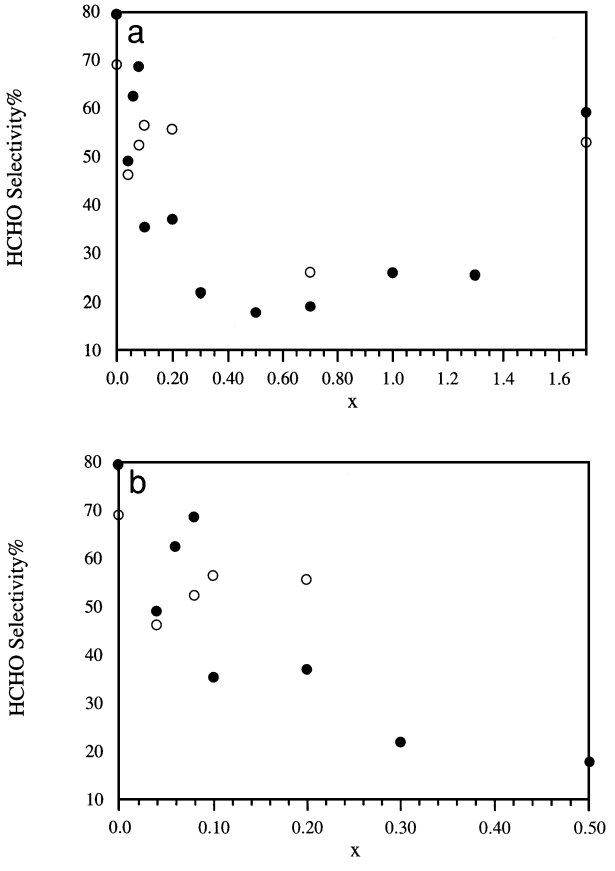

FIG. 6. The effect of Sb doping on catalyst selectivity to production of HCHO from methanol (at constant total conversion of <1%). Closed circles represent the selectivity of the catalysts after He/O_2 pretreatment and open circles represent the selectivity of the catalysts after He pretreatment (a) for a wide range of doping level, $x = 0$–1.7, and (b) expanded region $x = 0$–0.5.

GENERAL DISCUSSION

The general form of the activity/composition curve for these materials, i.e., an initial fall followed by a rise, has been observed for a range of other doped oxide materials (18–23). For example, the activity of model $Sn_{1-x}V_xO_2$ and $Ti_{1-x}V_xO_2$ catalysts in the decomposition of N_2O follows a similar pattern (18). This has been correlated with increases in the conductivity of the materials on doping (19). In addition, it is suggested that high selectivity to partial oxidation products is correlated with the resulting relatively facile electron exchange between active site cations, combined with a high metal–oxygen bond strength (i.e., strongly bound oxygen) (19). The latter property appears to be quite general to selective double oxide system; for example, the most selective systems show rather low rates of homomolecular isotopic oxygen exchange (24). This can be

rationalised on the basis of a Mars–van Krevelen type mechanism, where tightly bound nucleophilic lattice oxygen is responsible for production of selective oxidation products, whereas weakly bound, surface adsorbed electrophilic oxygen tends to lead to total oxidation (24).

In our previous work (22, 23), the activity of Sb-doped $SrSnO_3$ and Sb-doped $SrMoO_4$ catalysts in methanol oxidation followed a similar pattern. The activity and selectivity to formaldehyde was found to be strongly correlated with attainment of the bulk solubility limit of Sb in both the $SrSnO_3$ perovskite host and the $SrMoO_4$ scheelite host. In $SrSn_{1-x}Sb_xO_3$, we suggested that the minimum in activity and maximum in selectivity is associated with a maximum in the concentration of Sb^V–O bonds in the surface regions at around 10 at.% Sb doping. The high levels of Sb in the surface regions may also be sufficient to have a significant effect in isolating the deep oxidation centres, as in USb_3O_{10} (25, 26). This is combined with an increase in the electronic conductivity of the material as Sb is added, such that the material at 10% doping level combines centres of high metal–oxygen bond strength with quite high electron mobility, both important properties for high selectivity (19). In $SrMo_{1-x}Sb_xO_{4-\delta}$ the activity and selectivity to formaldehyde are functions of doping level and show a pronounced minimum at around the solubility limit of Sb, which is in the range 0.5–1% in these compounds. It was suggested that the replacement of Mo–O bonds with Sb^V–O (1.96 Å (22)) bonds which are weak bonds compared to Mo–O bonds (1.77 Å (27)) causes the selectivity goes down at lower doping level (∼0.5%) but since the selectivity for $SrMoO_4$ even at high temperature is 100%, any drop in selectivity is accompanied by a drop in total activity. So, at low doping level both activity and selectivity decrease (23).

Since different valence states for V are observed in $Bi_4V_2O_{11-\delta}$ (28), the redox flexibility of this element could be important in the catalytic cycle. In addition, the XPS study revealed the presence of Sb^V and vanadium in both V^{IV} and V^V valence states in the $Bi_4V_{1.5}Sb_{0.5}O_{10.7}$ compound (9, 28). Similar observations have been reported about the oxidation states of antimony and vanadium in $SrVO_4$ (12, 29, 30). Consistent with this, it appears that Sb^V is less reducible than V^V in octahedral coordination. By substituting Sb in $Bi_4V_2O_{11-\delta}$, V^V is replaced by Sb^V. In this case at lower doping level, $0 \le x \le 0.08$, the proportion of V^V in the materials goes down, and the materials become less reducible, and that leads to a drop in catalytic activity. It is accompanied by an increase in selectivity over the range $x = 0.06$–0.08. Comparing this range with Table 2, we see that the surface Sb concentration for samples in this range is probably high enough to produce tetragonal, rather than orthorhombic material at the surface. As the tetragonal phase shows higher conductivity (7), it may be possible that there is an enhanced surface conductivity at this point, contributing to the maximum in selectivity around $x = 0.08$.

The presence of V^{IV} in these materials is a consequence of effective reduction due to the presence of O vacancies. There is some suggestion in the literature that doping Sb onto V sites produces materials with large δ (i.e., high numbers of vacancies), and in turn, high $V^{IV}:V^V$ ratio (9). Thus, even though the Sb cation is formally isovalent with the V cation it substitutes for, some potential free carriers are produced in the form of V^{IV} sites on Sb-doping, through increasing O nonstoichiometry. However, Joubert *et al.* claimed that $Bi_4V_{1.5}Sb_{0.5}O_{10.7}$ is an electric insulator (9), because electronic carriers, i.e., small polarons (V^{IV} centres), are localised in this compound due to structural disorder in the perovskite layers. Consistent with this, it may be possible that by increasing the doping level in these materials, the proportion of localised small polarons (V^{IV} centres) increases without producing a sharp increase in electronic conductivity. The insulating nature of the bulk material, combined with increasing structural disorder may be responsible for the increase in activity in the $0.08 \le x \le 0.3$ region. Beyond the $x = 0.3$ level, the orthorhombic to tetragonal transition in the bulk causes an increase in conductivity (7) in the catalysts which tends to reduce the activity. In other words, the levelling in the rise of activity of the catalyst at this point may be due to this phenomenon. The sharp increase in activity of the catalysts at high doping level ($x > 1$) is coincident with the appearance of the second phase, which is unknown. This means that the catalysts containing the new phase are more active than the catalysts with single phase.

Pretreatment of the samples under a He stream could lead to creation of oxygen vacancies in the samples causing the conductivity of the compounds to increase, and removing any loosely bound surface O, and for these reason, the He/O_2 pretreated catalysts are more active than the He pretreated catalysts.

CONCLUSION

Ceramic model catalysts of formula $Bi_4V_{2-x}Sb_xO_{11-\delta}$ have been shown to be single phase over the composition range $0 \le x \le 0.3$, with a structural transition from orthorhombic to tetragonal at $x \sim 0.3$. This transition is also induced by reduction during the catalytic cycle. The activity and selectivity to production of formaldehyde, in methanol oxidation, of $Bi_4V_{2-x}Sb_xO_{11-\delta}$ catalysts are correlated with antimony doping level. XPS results show strong surface Sb segregation, and the presence of two oxidation states for vanadium, V^{IV} and V^V, in these materials. Therefore, it is suggested that the decrease in activity at lower doping level, $0 < x \le 0.08$, could be due to replacing V^V by Sb^V, causing the materials to become less reducible. The minimum in activity is combined with the maximum in selectivity of the antimony doped materials that is around $x = 0.08$. Beyond this level the activity climbs again. This could be due to

an increase in the proportion of V^{IV} and in the structural disorder within the peroskite layers. A change in the bulk structure of these catalysts, from orthorhombic to tetragonal, for $x > 0.3$ is reflected in a drop in the rate of increase of the activity in the $0.8 < x < 1$ range. The appearance of the unknown second phase is coincident with the sharp increase in activity of the materials at high doping level ($x > 1$).

ACKNOWLEDGMENT

This work was supported by EPSRC (UK) and the Research Institute of the Petroleum Industry of NIOC (National Iranian Oil Company).

REFERENCES

1. Wuzong, Z., Jefferson, D. A., Alario-Franco, M., and Thomas, J. M., *J. Phys. Chem*. **91**, 512 (1987).
2. Thomas, J. M., Ueda, W., Williams, J., and Harris, K. D. M., *Faraday Discuss. Chem. Soc.* **87**, 33 (1989).
3. Kargin, V. F., Kargin, Yu. F., and Skorikov, V. M., *Izv. Akad. Nauk SSSR, Neorg. Mater.* **20**(5), 815 (1984) in *Izv. Akad. Nauk SSSR, Neorg. Mater.* **23**(3), 523 (1987).
4. Barrault, J., Grosset, C., Dion, M., Ganne, M., and Tournoux, M., *Catalysis Lett.* **16**, 203 (1992).
5. Osipyan, V. G., Savchenko, L. M., Elbakyan, V. L., and Avakyan, P. B., *Izv. Akad. Nauk SSSR, Neorg. Mater.* **23**(3), 523 (1987).
6. Bush, A. A., Koshelayeva, V. G., and Venevtsev, Yu. N., *in* "Proceeding of the Sixth International Meeting on Ferroelectricity, Kobe 1985," *Jpn. J. Appl. Phys.* **24** (Suppl. 24-2), 625 (1985).
7. Abraham, F., Boivin, J. C., Mairesse, G., and Nowogrocki, G., *Solid State Ionics* **40/41**, 934 (1990).
8. Iharada, T., Hammouche, A. Fouletier, J., and Kleitz, M., *Solid State Ionics* **48**, 257 (1991).
9. Joubert, O., Jouanneaux, A., Ganne, M., and Toumoux, M., *Mater. Res. Bull.* **27**, 1235 (1992).
10. Lee, C. K., Bay, B. H., and West, A. R., *J. Mater. Chem*. **6**(3), 331 (1996).
11. Berry, F. J., and Brett, M. E., *J. Catal.* **88**, 232 (1984).
12. Nilsson, R., Lindblad, T., Andersson, A., Song, C., and Hansen, S., *Stud. Surf. Sci. Catal.* **82**, 293 (1994).
13. British patent 1324693 (1973).
14. British patent 1336136 (1973).
15. British patent 1363455 (1974).
16. British patent 1377211 (1974).
17. Mendialua, J., Casanova, R., and Barbaux, Y., *J. Electron Spectrosc. Related Phenom*. **71**, 249 (1995).
18. Pomonis, P., and Vickerman, J. C., *J. Catal.* **90**, 305 (1984).
19. Pomonis, P., and Vickerman, J. C., *J. Catal.* **55**, 88 (1978).
20. Pomonis, P. J., and Vickerman, J. C., *Faraday Discuss. Chem. Soc.* **72**, 247 (1981).
21. Vickerman, J. C., *in* "Catalysis" (C. Kemball and D. A. Dowden, Eds.), Vol. 2 (specialist periodical report), p. 107. Chemical Society, London, 1987.
22. Aghabozorg, H. R., Sakakini, B. H., Roberts, A. J., Vickerman, J. C., and Flavell, W. R., *Catal. Lett.* **39**, 9 (1991).
23. Aghabozorg, H. R., Flavell, W. R., and H. R., Sakakini, B. H., manuscript in preparation.
24. Bielanski, A., and Haber, J., "Oxygen in Catalysis," p. 132. Dekker, New York, 1991, and references therein.
25. Grasselli, R. K., and Suresh, D. D., *J. Catal.* **25**, 273 (1972).
26. Grasselli, R. K., and Burrington, J. D., *Adv. Catal.* **30**, 133 (1981).
27. Brazdil, J. F., Glaser, L. C., and Grasselli, R. K., *J. Catal.* **81**, 142 (1983).
28. Joubert, O., Jouanneaux, A., and Ganne, M., *Mater. Res. Bull.* **29**(2), 175 (1994).
29. Birchall, T., and Sleight, A. W., *Inorg. Chem*. **15**(4), 868 (1976).
30. Nilsson, R., Lindblad, T., and Andersson, A., *J. Catal.* **148**, 510 (1994).
31. Bhattacharya, A. K., Mallick, K. K., and Thomas, P. A., *Solid State Commun.* **91**(5), 357 (1994).
32. Pernot, E., Anne, M., Bacmann, M., Strobel, P., Fouletier, J., Vannier, R. N., Mairesse, G., Abraham, F., and Nowogrock, G., *Solid State Ionics* **70/71**, 259 (1994).